Available online at www.sciencedirect.com
ScienceDirect
International Journal of Heat and Mass Transfer 51 (2008) 4759–4774
International Journal of HEAT and MASS TRANSFER
www.elsevier.com/locate/ijhmt

Multicomponent-liquid–fuel vaporization with complex configuration

William A. Sirignano *, Guang Wu

Department of Mechanical and Aerospace Engineering, University of California, Irvine, CA 92697-3975, United States

Received 12 September 2007; received in revised form 13 February 2008
Available online 11 April 2008

Abstract

An analysis is presented for multicomponent-liquid–fuel vaporization in a general geometrical situation, e.g., a dense spray. Variable transport properties and only Stefan flow are considered. The problem is separated, using a mass-flux potential function, into a one-dimensional problem for the quasi-steady, gas-phase scalar properties and a three-dimensional problem for the mass-flux potential. The theory predicts scalar gas-phase profiles and vaporization rates for any value of the Lewis number. Transient heat- and mass-diffusion in the liquid interiors is considered with special attention given to the fast- and slow-diffusion limits. Eight droplets in a cubic array are considered in the calculations with a blended liquid mixture of heptane, octane, and decane. Comparisons are made amongst the results for the various liquid-diffusion models: transient behavior, the fast-vaporization limit, and the slow-vaporization limit.

Keywords: Multicomponent; Transient vaporization/heating; Droplet arrays

1. Introduction

In previous papers on single-component liquids [1–4], liquid–fuel vaporization and burning for general configurations, including dense droplet arrays and liquid films, has been analyzed. Those works built upon the works by Labowsky [5–7], Umemura et al. [8,9], and Brzustowski and coworkers [10,11]. Labowsky [6,7] introduced the mass-flux potential function (which we apply later), first transformed the field equation to Laplace's equation, and examined up to nine droplets. He used the method of images. In a series of papers, Imaoka and Sirignano explored and compared different computational approaches [1], extended the capability to handle transient as well as quasi-steady cases [2,3], calculated arrays as large as 1000 droplets [3], considered effects of non-uniform initial droplet size and initial spacing amongst droplets [2,3], demonstrated the proper procedure for the averaging of the gas-phase transport properties, and obtained correlations based on similarity variables [1,3] that can be used in lieu of detailed calculations in the future.

Except for Sirignano [4], the above researches were limited to cases with unitary values of Lewis number. Sirignano recently analyzed the case of many droplets and/or liquid films with Fickian diffusion and non-unitary Lewis numbers. The mass diffusivities differed according to the diffusing species and varied with the spatial location.

In similar fashion to the above references, we will focus here on situations with only Stefan convection and without forced or natural convection. We assume that the Stefan convection at the surface is sufficiently strong to cause the gas velocity to be normal to the liquid–gas interface at that surface. Chemical reactions will not be considered. There will be $N-2$ miscible components in the liquid-phase, all of which produce vapors. In addition, oxygen and nitrogen will be present in the gas with nitrogen concentration dominant amongst the N gas species. The Lewis number will be allowed to vary over the field.

In our analysis, we will resolve both the gas-phase and liquid-phase properties, balancing mass and energy fluxes at the phase interfaces. So, this analysis and those cited above fit the category of array theory but not the group

* Corresponding author. Tel.: +1 949 824 3700; fax: +1 949 824 3773.
E-mail address: sirignan@uci.edu (W.A. Sirignano).

0017-9310/$ - see front matter © 2008 Elsevier Ltd. All rights reserved.
doi:10.1016/j.ijheatmasstransfer.2008.02.018

Nomenclature

Latin letters

B_M	Spalding mass-transfer number
B_H	Spalding heat-transfer number
c_p	constant pressure specific heat
D	diffusion coefficient
h	specific enthalpy
L	latent heat of vaporization
L_{eff}	effective latent heat of vaporization
Le	Lewis number
$\dot{m}$	mass vaporization rate
N	number of droplets or mole number
$\dot{q}$	magnitude of heat flux
r	radial coordinate
R	droplet radius or universal gas constant
T	temperature
T_b	boiling temperature
$\vec{V}$	mass-averaged velocity vector
W	molecular weight
X	mole fraction
Y	mass fraction

Greek letters

α	thermal diffusivity
ϵ	mass-flux fraction
ζ	normalized radial coordinate
η_A	interactive-isolated vaporization ratio
λ	thermal conductivity
ρ	density
ϕ	potential function
Φ	normalized potential function
ξ	similarity parameter

Subscripts

∞	ambient value
ϵ	mass-flux-averaged value
0	initial value
eff	effective value
iso	isolated-droplet
l	liquid-phase
S	surface value
lS	liquid surface
n	the nth species

Superscript

bar	average over gas-phase

theory category as these categories are defined by Sirignano [12]. So, this work differs from studies such as the famous work by Chiu et al. [13] in that the Nusselt and Sherwood numbers for each droplet are not prescribed here but rather are determined. This is the first analysis of multicomponent-liquid vaporization using array theory.

2. Quasi-steady, gas-phase equations

Standard notation will be used. In respective order, ρ, $\vec{V}$, and T represent density, vector velocity of the gas mixture, and temperature; $\vec{V}_n$, Y_n, and h_n represent vector diffusion velocity, mass fraction, and specific enthalpy, all for species n; D, λ, and c_p represent coefficients for mass diffusivity, thermal conductivity, and specific heat at constant pressure. Other variables are defined as they are introduced.

The quasi-steady gas-phase conservation equations for energy, mass, and species mass are given in Eqs. (1)–(9) of Sirignano [4]. Here, we neglect the reaction terms and the heats of formation in those equations. Fickian diffusion is assumed. Since the gas mixture is dominated by nitrogen gas, each D_n is the binary diffusion coefficient for that nth species with nitrogen. The nitrogen mass fraction can be determined from the other mass fractions knowing that all mass fractions sum to unity. Radiation, kinetic energy and viscous dissipation are neglected. The momentum equation will be replaced by a uniform-pressure assumption which is consistent with neglect of terms of order Mach number squared and of order Mach number squared divided by Reynolds number when compared to unity.

The mass-flux potential is used following Labowsky [6,7], Umemura et al. [8,9], Imaoka and Sirignano [1–3]. Imaoka and Sirignano [2] have shown that an irrotational velocity field and the alignment of the diffusive-flux vector with or directly against the local velocity vector are sufficient conditions for a mass-flux potential ϕ to exist; i.e., $\rho\vec{V} = \nabla\phi$. This implies that gradients of the scalar properties are parallel locally with the mixture velocity $\vec{V}$; diffusion velocity V_n and mixture velocity are accordingly aligned. With the liquid surface at a uniform temperature, the gas velocity at the surface must be orthogonal to the surface. This type of flow can be expected without forced convection or natural convection and subsequent shear flows. Consistent with the previous assumptions, the mass-flux potential allows for a general solution to the flow.

When the scalar gradients and velocity are parallel locally, we can conveniently use the normalized mass-flux fraction ϵ_n where $\rho\vec{V}\epsilon_n = \rho\vec{V}Y_n - \rho D_n \nabla Y_n$. For the quasi-steady, gas-phase behavior, the ϵ_n are constant along a streamline. ϵ_n will be zero for the non-vaporizing oxygen and nitrogen and a positive number exists for each of the vaporizing species with $\sum_{n=1}^{N}\epsilon_n = \sum_{n=1}^{N-2}\epsilon_n = 1$. It is convenient to define a mass-flux-weighted specific sensible enthalpy h_ϵ and a mass-flux-weighted specific heat $c_{p,\epsilon}$ such that

$$h_\epsilon = \sum_{n=1}^{N} \epsilon_n h_n = \sum_{n=1}^{N-2} \epsilon_n \int c_{p,n}\,\mathrm{d}T = \int \left(\sum_{n=1}^{N-2} \epsilon_n c_{p,n} \right) \mathrm{d}T = \int c_{p,\epsilon}\,\mathrm{d}T. \quad (1)$$

With known ϵ_n values, h_ϵ is a function only of temperature, making it more convenient than the mass-weighted specific sensible enthalpy $h = \sum_{n=1}^{N} Y_n h_n =$ which varies with both mass fractions and temperature. Mass-flux-weighted (and mole-flux-weighted) enthalpy has been used for more than one-half of a century in the transport, combustion, and vaporizing-droplet literatures [14,15]. It was also used by Law and Law [16] for their non-unitary-Lewis number, single-droplet work. However, new importance for it is identified by Sirignano [4]. This enthalpy function allows the proper (natural) definitions of Lewis number and averaged transport properties across the field and the formation of a constraint on the surface temperature and surface heat flux.

The boundary conditions at the liquid–gas interface for the mass fluxes of the $N-2$ vaporizing species become

$$\rho \vec{V} \epsilon_n \cdot \vec{e} = (\rho \vec{V} Y_n - \rho D_n \nabla Y_n) \cdot \vec{e} = \rho (\vec{V} + \vec{V}_n) \cdot \vec{e} Y_n, \quad n = 1, 2, \ldots, N-2 \quad (2)$$

and, for the non-vaporizing oxygen and nitrogen,

$$(\rho \vec{V} Y_n - \rho D_n \nabla Y_n) \cdot \vec{e} = \rho (\vec{V} + \vec{V}_n) \cdot \vec{e} Y_n = 0, \quad n = N-1, N, \quad (3)$$

where $\vec{e}$ is the unit normal vector at the liquid–gas interface. With the assumption that the velocity and the scalar gradients at that interface are normal to the surface, Eqs. (2) and (3) are consistent with the definition of ϵ_n.

3. Integration of the gas-phase equations

Define the quantity H such that $\rho \vec{V} H = \rho \vec{V} h_\epsilon - \lambda \nabla T$. As shown by Sirignano [4], H will not vary along a streamline. With neglect of radiation, the energy-balance boundary condition at the liquid–gas interface is

$$\lambda (\nabla T) \cdot \vec{e} = \rho \vec{V} \cdot \vec{e} L + q_l = \rho \vec{V} \cdot \vec{e} L_{\mathrm{eff}}, \quad (4)$$

where $L_{\mathrm{eff}} = L + \dot{q}_l / (\rho \vec{V} \cdot \vec{e})$ contains the effect of both the latent heat L and the heat flux to the liquid interior $\dot{q}_l$. With the velocity and the scalar gradients at that interface normal to the surface, we can obtain that $H = h_{\epsilon,S} - L_{\mathrm{eff}} = \sum_{n=1}^{N} \epsilon_n h_{n,S} - L_{\mathrm{eff}}$, where the subscript S denotes the gas property at the liquid–gas surface.

We can conclude from the definitions of ϵ_n, H, and ϕ that

$$\rho \vec{V} = \nabla \phi = \frac{\lambda \nabla T}{h_\epsilon - H} = \frac{(\lambda / c_{p,\epsilon}) \nabla h_\epsilon}{h_\epsilon - H} = \frac{\rho D_n \nabla Y_n}{Y_n - \epsilon_n}, \quad n = 1, \cdots, N. \quad (5)$$

So, logarithmic forms naturally appear for h_ϵ and Y_n. Also, the scalar variables are one-dimensional, i.e., functions only of ϕ, consistent with the previous results of Imaoka and Sirignano for $Le = 1$. Assume the same scalar value exists at any point on the liquid–gas interface. Then, integrals can readily be obtained for these scalars:

$$\frac{h_\epsilon - H}{h_{\epsilon,\mathrm{ref}} - H} = \mathrm{e}^{\int_{\phi_{\mathrm{ref}}}^{\phi} \mathrm{d}\phi' / (\lambda / c_{p,\epsilon})}, \quad \frac{Y_n - \epsilon_n}{Y_{n,\mathrm{ref}} - \epsilon_n} = \mathrm{e}^{\int_{\phi_{\mathrm{ref}}}^{\phi} \mathrm{d}\phi' / (\rho D_n)}. \quad (6)$$

Reference values are taken at the liquid–gas interface or infinity. T_∞ and $Y_{n,\infty}$ are given at infinity; for the vaporizing species, consider $Y_{n,\infty} = 0$. The continuity equation is replaced by

$$\nabla^2 \phi = 0 \quad (7)$$

with the boundary conditions at infinity and at the droplet/gas interface. ϕ_∞ remains to be determined. $\phi = \phi_S$ at the liquid–gas interface will be conveniently chosen to be zero which removes the arbitrariness introduced with the definition of the potential function. Note that the $\phi = \phi_S = 0$ surface is not simply connected in the general case where more than one droplet exists in the array.

Take the reference value at the liquid interface for the vaporizing species so that

$$\frac{Y_n - \epsilon_n}{Y_{n,S} - \epsilon_n} = \mathrm{e}^{\int_0^{\phi} \mathrm{d}\phi' / (\rho D_n)}. \quad (8)$$

We can now determine ϕ_∞ and allow normalization of the potential function. Define

$$\Phi = \frac{\phi}{\phi_\infty}; \quad \overline{\rho D_n} = \left[\int_0^1 \mathrm{d}\Phi' / (\rho D_n) \right]^{-1}; \quad \overline{\lambda / c_{p,\epsilon}} = \left[\int_0^1 (c_{p,\epsilon} / \lambda)\,\mathrm{d}\Phi' / \right]^{-1} \quad (9)$$

for any integer value of n where $0 \leqslant \Phi \leqslant 1$ and the overline defines a spatially averaged value. Then, using Eq. (8) at infinity, we obtain

$$\phi_\infty = \overline{\rho D_n} ln \left[\frac{\epsilon_n}{\epsilon_n - Y_{n,S}} \right] = \overline{\rho D_n} ln [1 + B_{M,n}], \quad (10)$$

where the Spalding mass-transfer number for each vaporizing species is given by

$$B_{M,n} = \frac{Y_{n,S}}{\epsilon_n - Y_{n,S}}. \quad (11)$$

The value of the potential function at infinity is the integral of the mass-flux (per unit area) over any streamline. ϕ_∞ is independent of n so that Eq. (10) implies $N-3$ relationships amongst the $N-2$ values for the ϵ_n for vaporizing species. Together with the condition that $\sum_{n=1}^{N-2} \epsilon_n = 1$, there are $N-2$ relations which determine the values of ϵ_n.

Now, from Eqs. (8)–(10), we obtain

$$\frac{Y_n - \epsilon_n}{Y_{n,S} - \epsilon_n} = [1 + B_{M,n}]^{\overline{\rho D_n} \int_0^{\Phi} \mathrm{d}\Phi' / (\rho D_n)}. \quad (12)$$

For each vaporizing species, a phase-equilibrium constraint at the liquid surface will prescribe $Y_{n,S}$ as a function of the surface temperature T_S. We will use for our calculations a

Clausius–Clapeyron relation together with Raoult's law [12] so that

$$Y_{n,\mathrm{S}} = \frac{W_n X_{n,\mathrm{lS}} \sum_{k=1}^{N} (Y_{k,\mathrm{S}}/W_k)}{p} \mathrm{e}^{L_n/RT_{b,n}} \mathrm{e}^{-L_n/RT_{\mathrm{S}}}; \quad n = 1, \ldots, N-2, \tag{13}$$

where $T_{b,n}, W_n, L_n$, and $X_{n,\mathrm{lS}}$ are the boiling temperature (a function of pressure), molecular weight, latent heat of vaporization, and liquid mole fraction at the surface for vaporizing species n.

Once T_{S} and $X_{n,\mathrm{lS}}$ are known, the above solutions will allow the determination of the gas-phase field properties as a function of the mass-flux potential function. We will proceed in this section to obtain those solutions. In subsequent sections, we will determine the mass-flux potential as a function of position in space and will study the internal transient heat- and mass-diffusion processes that constrain the values of T_{S} and $X_{n,\mathrm{lS}}$.

For the oxygen species, a reference value at infinity is more convenient. Since $\epsilon_{\mathrm{O}_2} = 0$, we obtain from Eq. (6)

$$\frac{Y_{\mathrm{O}_2}}{Y_{\mathrm{O}_2,\infty}} = \mathrm{e}^{\int_{\phi_\infty}^{\phi} \mathrm{d}\phi'/(\rho D_{\mathrm{O}_2})} = \mathrm{e}^{\phi_\infty \int_1^{\Phi} \mathrm{d}\Phi'/(\rho D_{\mathrm{O}_2})}. \tag{14}$$

As mentioned above, the nitrogen mass fraction is calculated using global continuity, i.e.,

$$Y_{\mathrm{N}_2} = 1 - Y_{\mathrm{O}_2} - \sum_{n=1}^{N-2} Y_n. \tag{15}$$

Now, we can examine the temperature field using Eq. (6) with the reference value at the liquid/gas interface.

Define

$$B_{\mathrm{H},\epsilon} = \frac{\sum_{n=1}^{N-2} \epsilon_n [h_{n,\infty} - h_{n,\mathrm{S}}]}{L_{\mathrm{eff}}} = \frac{[h_{\epsilon,\infty} - h_{\epsilon,\mathrm{S}}]}{L_{\mathrm{eff}}}. \tag{16}$$

From Eqs. (6), (9), and (16), we obtain

$$\phi_\infty = \overline{\lambda/c_{p,\epsilon}} ln \frac{[h_{\epsilon,\infty} - h_{\epsilon,\mathrm{S}} + L_{\mathrm{eff}}]}{L_{\mathrm{eff}}} = \overline{\lambda/c_{p,\epsilon}} ln[1 + B_{\mathrm{H},\epsilon}]. \tag{17}$$

Then, Eq. (6) can be rewritten as

$$\begin{aligned} \frac{h_\epsilon - h_{\epsilon,\mathrm{S}} + L_{\mathrm{eff}}}{L_{\mathrm{eff}}} &= \mathrm{e}^{\phi_\infty \int_0^{\Phi} \mathrm{d}\Phi'/(\lambda/c_{p,\epsilon})} \\ &= \mathrm{e}^{\overline{\lambda/c_{p,\epsilon}} ln[1+B_{\mathrm{H},\epsilon}] \int_0^{\Phi} \mathrm{d}\Phi'/(\lambda/c_{p,\epsilon})} \\ &= [1 + B_{\mathrm{H},\epsilon}]^{\overline{\lambda/c_{p,\epsilon}} \int_0^{\Phi} \mathrm{d}\Phi'/(\lambda/c_{p,\epsilon})} \\ &= \mathrm{e}^{\overline{\rho D_n} \ln[1+B_{\mathrm{M},n}] \int_0^{\Phi} \mathrm{d}\Phi'/(\lambda/c_{p,\epsilon})} \\ &= [1 + B_{\mathrm{M},n}]^{\overline{\rho D_n} \int_0^{\Phi} \mathrm{d}\Phi'/(\lambda/c_{p,\epsilon})}. \end{aligned} \tag{18}$$

Note that any value of n may be used be in Eq. (18) in accordance with Eq. (10).

We define a new average Lewis number here for each species diffusing through the nitrogen: $Le_{\epsilon,n} = (\overline{\lambda/c_{p,\epsilon}})/(\overline{\rho D_n})$. Realize that, because of the use of a mass-flux-weighted specific heat rather than a mass-weighted specific heat, the $Le_{\epsilon,n}$ here is different from the Lewis number presented in other literature, except for the case where species specific heats have the same value. So, a unitary-Lewis number situation with mass-weighted mixture properties in the other literature need not be a unitary-Lewis number situation with the mass-flux-weighted specific heat used here.

For the purpose of calculations, specific enthalpies for each species can be expressed as functions of temperature using the NASA polynomials in the appendix of Ref. [17]. Once the interface temperature T_{S}, interface liquid mole fraction $X_{n,\mathrm{lS}}$, and mass-flux fractions ϵ_n are known, Eqs. (12)–(15) and (18) determine the gas-phase scalar fields as functions of the potential function.

4. Constraint on the liquid surface temperature

From Eq. (18) and the definition of the average Lewis number, we find that

$$[1 + B_{\mathrm{M},n}]^{1/Le_{\epsilon,n}} = 1 + B_{\mathrm{H},\epsilon}. \tag{19}$$

Eq. (19) holds for any value of the index n (i.e., any vaporizing species) while the right-hand side does not vary with n. So,

$$[1 + B_{\mathrm{M},j}]^{1/Le_{\epsilon,j}} = [1 + B_{\mathrm{M},k}]^{1/Le_{\epsilon,k}}. \tag{20}$$

This means that the particular function of mass-transfer number and Lewis number is the same for any two values j, k of the parameter n. Also, we can say that

$$[1 + B_{\mathrm{M},j}] = [1 + B_{\mathrm{M},k}]^{Le_{\epsilon,j}/Le_{\epsilon,k}} = [1 + B_{\mathrm{M},k}]^{\overline{\rho D_k}/\overline{\rho D_j}}. \tag{21}$$

Obviously, if the mass diffusivity is the same for any two species, their $B_{\mathrm{M},n}$ values are identical. For the case where all gas-phase diffusivities for the vaporizing species are equal, then all $B_{\mathrm{M},n}$ values are identical and Eqs. (11) and (21) yield the $N-3$ relations

$$\epsilon_1/Y_{1,\mathrm{S}} = \epsilon_2/Y_{2,\mathrm{S}} = \cdots = \epsilon_{N-2}/Y_{N-2,\mathrm{S}}. \tag{22}$$

Given that $\sum_{k=1}^{N-2} \epsilon_k = 1$ and $\sum_{k=1}^{N} Y_{k,S} = 1$, Eq. (22) yields

$$\epsilon_n = \frac{Y_{n,\mathrm{S}}}{\sum_{k=1}^{N-2} Y_{k,\mathrm{S}}}; \quad n = 1, 2, \ldots, N-2. \tag{23}$$

Furthermore, Eq. (19) can be recast using Eqs. (4) and (16) as

$$L_{\mathrm{eff}} = L + \frac{\dot{q}_{\mathrm{l}}}{\rho \vec{V} \cdot \vec{e}} = \frac{h_{\epsilon,\infty} - h_{\epsilon,\mathrm{S}}}{B_{\mathrm{H},\epsilon}} = \frac{h_{\epsilon,\infty} - h_{\epsilon,\mathrm{S}}}{[1 + B_{\mathrm{M},n}]^{1/Le_{\epsilon,n}} - 1}. \tag{24}$$

This equation can be considered as a boundary condition at the liquid–gas interface for transient heating of the liquid. When conduction to the liquid interior ceases (i.e., $q_{\mathrm{l}} = 0$), the relationship together with the phase-equilibrium relationship prescribes the wet-bulb liquid temperature, $T_{\mathrm{S}} = T_{\mathrm{wb}}$.

In the case where specific heats are identical for all species, including oxygen and nitrogen, we have $h_\epsilon = h$,

$h_{\epsilon,\infty} = h_\infty, h_{\epsilon,\mathrm{S}} = h_\mathrm{S}$, and $Le_\epsilon = Le$ (the classical Lewis number). The result is

$$B_{\mathrm{H}\epsilon} = \frac{h_\infty - h_S}{L_{\mathrm{eff}}} = B_\mathrm{H}, \tag{25}$$

where B_H is the classical heat-transfer number proposed by Spalding.

Remarkably, the liquid surface boundary conditions given by Eqs. (13) and (24) are independent of the geometrical configuration (e.g., shape of liquid surfaces or number of droplets).

In the case where no heating of the liquid interior occurs, $L_{\mathrm{eff}} = L$ and Eq. (19) becomes

$$\frac{L + \sum_{k=1}^{N-2} \epsilon_k [h_{k,\infty} - h_{k,\mathrm{S}}]}{L} = \left[\frac{\epsilon_n}{\epsilon_n - Y_{n,\mathrm{S}}}\right]^{1/Le_{\epsilon,n}} \tag{26}$$

for any value of n. This relationship determines, together with the phase-equilibrium relations that relate $Y_{n,\mathrm{S}}$ to T_S and the equations of state that relate h_n to T, the value for the surface temperature T_S. This value, which is expected asymptotically in time after liquid heating ceases, is named the wet-bulb temperature T_{wb}.

5. Determination of the mass-flux potential

From Eqs. (7) and (9), and the selection of the arbitrary constant, we have

$$\nabla^2 \Phi = 0; \quad \Phi_\mathrm{S} = 0; \quad \Phi_\infty = 1. \tag{27}$$

For a given geometrical description of the liquid surfaces, Φ can be determined as a function of position in space. There is no explicit dependence on liquid–fuel choice, transport properties, and scalar boundary values; these parameters only appear through the normalization factor. So, the solution for Φ will be identical to solutions obtained in the previous unitary-Lewis number studies of Imaoka and Sirignano [1–3].

6. Determination of the vaporization rate

We will follow the approach developed in previous papers [1–4]. The vaporization rate is equal to the mass-flux leaving the liquid surface. So, integrating over all of the liquid surfaces, we obtain the global vaporization rate. With only spherical droplets, the non-dimensional vaporization rate for the jth droplet is

$$\eta_j = \frac{\dot{m}_j}{\dot{m}_{j,\mathrm{iso}}} = \frac{\overline{\rho D_n} \ln[1 + B_{\mathrm{M},n}]}{\dot{m}_{j,\mathrm{iso}}} \int_{S_j} \int \nabla \Phi \cdot \vec{e}\, \mathrm{d}S$$
$$= \frac{1}{4\pi R_j} \int_{S_j} \int \nabla \Phi \cdot \vec{e}\, \mathrm{d}S, \tag{28}$$

where R_j and $\dot{m}_{j,\mathrm{iso}}$ are the instantaneous droplet radius and the instantaneous vaporization rate, respectively, for a droplet of the same radius but isolated from other droplets. S_j is the surface area of the jth droplet. It is known [12] that, for an isolated spherical droplet, $\dot{m}_{j,\mathrm{iso}} = 4\pi \overline{\rho D_n} R \ln[1 + B_{\mathrm{M},n}] = 4\pi \overline{(\lambda/c_{p,\epsilon})} R \ln(1 + B_{\mathrm{H}f,\epsilon})$ which has been used above.

The isolated-droplet vaporization rate depends upon the values of the Lewis number and transport properties. For example, the value of $\overline{\rho D_n}$ is directly affected by transport-property values while the value of $B_{\mathrm{M},n}$ is indirectly affected by the relationship between the liquid surface temperature and transport properties.

Normalizations of lengths appearing in Eq. (7) will show that the results for η_j are independent of the choice of the reference length. This means that η_j will depend only on length ratios, e.g., droplet-diameter-to-droplet-spacing ratio, and not on actual size. So, if all lengths are scaled upwards or downwards in proportion, η_j will not change in value.

The average non-dimensional vaporization rate for a droplet array of $\overline{N}$ droplets can be found as $\eta_\mathrm{A} = (\sum_{j=1}^{\overline{N}} \eta_j)/\overline{N}$.

In these non-dimensional forms, the vaporization rates η_j and η_A are independent of liquid–fuel choice, transport properties, and scalar boundary conditions. They depend only on geometrical configuration so that previous computational results can be employed. In particular, the computational correlation $\eta(\xi)$ of Imaoka and Sirignano [1,3] can be used. That is,

$$\eta_\mathrm{A} = 1 - \frac{1}{1 + 0.725671 \xi^{0.971716}};$$
$$\xi = \frac{\left[\frac{4\pi V_\mathrm{A} \overline{N}}{3 V_\mathrm{l}}\right]^{1/3}}{[\overline{N}^{1/3} - 1]\overline{N}^{0.72}}, \tag{29}$$

where $V_\mathrm{A}, V_\mathrm{l}$, and $\overline{N}$ are the array volume, total liquid volume, and droplet number, respectively. So, if only vaporization rates are desired, it is not necessary to solve Eq. (27) since Eq. (29) contains results from Eq. (27).

Eq. (29) and much of the previous formulation apply only if every droplet has the same instantaneous surface temperature. That assumption will not hold during transient heating of a large, closely-packed array where the inner droplets are given heat protection by the outer droplets. Our analysis here will exclude those cases where temperature varies along the interfaces.

For a spherical droplet in a situation where all droplets are equi-sized, it follows that

$$\dot{R} = -\frac{\eta_\mathrm{A}}{\rho_\mathrm{l} R} \frac{\overline{\lambda}}{c_{p,\epsilon}} \ln(1 + B_{\mathrm{H},\epsilon}) = -\frac{\eta_\mathrm{A}}{\rho_\mathrm{l} R} \overline{\rho D_n} \ln(1 + B_{\mathrm{M},n}). \tag{30}$$

7. Liquid heating and mixing

The heat and mass diffusivities in the liquid are much smaller than the counterpart gas-phase values. So, the gas-phase can be treated as quasi-steady although transient effects and time-derivative terms must be considered for the liquid. Spherically symmetric diffusion in the droplets will be an approximation. We will consider the liquid-phase properties to be constant throughout the liquid and that

all droplets have the same instantaneous size, temperature, and composition. This will have implications about the droplet-array configuration. First, we will discuss a general situation of transient behavior where heat and mass-diffusion times droplet lifetimes are of the same order of magnitude. Then, in later subsections, we consider special asymptotic cases where one characteristic time can be considered small compared to another characteristic time.

7.1. Transient behavior

The governing equations for liquid-phase diffusion are

$$\frac{\partial T_l}{\partial t}=\frac{1}{\rho_l c_l r^2}\frac{\partial\left(\lambda_l r^2\frac{\partial T_l}{\partial r}\right)}{\partial r};\quad \frac{\partial Y_{l,n}}{\partial t}=\frac{1}{r^2}\frac{\partial\left(D_{l,n}r^2\frac{\partial Y_{l,n}}{\partial r}\right)}{\partial r}. \tag{31}$$

c_l, ρ, λ_l, and $D_{l,n}$ are specific heat, density, thermal diffusivity, and mass diffusivity in the liquid-phase. r is the radial position in a droplet.

Note that some controversy exists about the proper form of the mass-diffusion equation for multicomponent liquids. There are questions about the proper formulation of the diffusion velocity and its relationship to the gradient(s) of partial density or molar concentration. So, Eq. (31) should be viewed as an approximation. Note further that no advective term is included which implies that all components are approximated to have the same density. Otherwise, mass-diffusion would be accompanied by a change in total density, implying mean mass motion.

The interface is regressing into the liquid due to vaporization. So, these equations are part of a moving-boundary problem. A transformation to a fixed-boundary problem is desirable and will now be made. Define $\zeta = r/R(t)$ where $R(t)$ is the instantaneous droplet radius. Then, following established methods [12], the liquid-phase diffusion equations transform to

$$\frac{\partial T_l}{\partial t}=\frac{\alpha_l}{R^2}\frac{\partial^2 T_l}{\partial\zeta^2}+\left[\frac{2\alpha_l}{R^2\zeta}+\frac{\zeta\dot{R}}{R}\right]\frac{\partial T_l}{\partial\zeta}+\frac{1}{\rho_l c_l R^2}\frac{\partial\lambda_l}{\partial\zeta}\frac{\partial T_l}{\partial\zeta} \tag{32}$$

and

$$\frac{\partial Y_{l,n}}{\partial t}=\frac{D_{l,n}}{R^2}\frac{\partial^2 Y_{l,n}}{\partial\zeta^2}+\left[\frac{2D_{l,n}}{R^2\zeta}+\frac{\zeta\dot{R}}{R}\right]\frac{\partial Y_{l,n}}{\partial\zeta}+\frac{1}{R^2}\frac{\partial D_{l,n}}{\partial\zeta}\frac{\partial Y_{l,n}}{\partial\zeta}. \tag{33}$$

Initial conditions, symmetry boundary conditions at the droplet center, and interface boundary conditions on these equations are

$$\begin{aligned}
&T_l(\zeta,t=0)=T_{l0};\quad \frac{\partial T_l}{\partial\zeta}(\zeta=0,t)=0;\\
&Y_{l,n}(\zeta,t=0)=Y_{l,n0};\quad \frac{\partial Y_{l,n}}{\partial\zeta}(\zeta=0,t)=0;\\
&\lambda_l\frac{\partial T_l}{\partial\zeta}(\zeta=1,t)=-\rho_l R\dot{R}\left[\frac{\sum_{k=1}^{N-2}\epsilon_k(h_{k,\infty}-h_{k,S})}{(1+B_{M,n})^{1/Le_{\epsilon,n}}-1}-\sum_{k=1}^{N-2}\epsilon_k L_k\right];\\
&\epsilon_n=Y_{l,n}(\zeta=1,t)+\frac{D_{l,n}}{R\dot{R}}\frac{\partial Y_{l,n}}{\partial\zeta}(\zeta=1,t).
\end{aligned} \tag{34}$$

The last two conditions above apply at the interface which is a fixed point in ζ space. The fifth condition is a consequence of Eq. (24); and the final condition reflects the fact the total vaporization rate of species n is the sum of an advective flux (in a reference frame fixed to the regressing surface) and a diffusive-flux.

Eqs. (11), (13), and (21), together with the relation $\sum_{k=1}^{N-2}\epsilon_k=1$, yield the mass-flux fractions ϵ_n as functions of temperature and liquid mole fractions at the surface. Note that, when all mass diffusivities are identical, Eq. (22) replaces Eq. (21). Furthermore, (32)–(34), together with $X_{l,n}=[Y_{l,n}/W_n]/[\sum_{k=1}^{N-2}(Y_{l,k}/W_k)]$ describe the mole fractions and temperature inside the liquid (including surface values) as functions of the ϵ_n values. So, together, these equations form a system which can be solved to give the results for a general case with a transient liquid-phase and a quasi-steady gas-phase.

We will specialize now with two limiting cases: very fast-vaporization and very slow-vaporization.

7.2. Fast-vaporization limit

Consider now a situation where the regression rate of the interface $\dot{R}$ is much greater than both the time for heat-diffusion and the time for mass-diffusion across the droplet: i.e., $R\dot{R}/\alpha_l \gg 1$ and $R\dot{R}/D_{l,n} \gg 1$. As explained by Sirignano [12], thin quasi-steady layers for thermal and mass-diffusion form in the liquid adjacent to the surface in this limit. There are diffusive-convective and diffusive-advective balances in these layers. The result is that, from the thermal balance,we find that

$$L_{\text{eff}}=L+c_l[T_{l,S}-T_{l0}]=L+c_l[T_S-T_{l0}]. \tag{35}$$

For the mass balance, we have that the mass-flux fractions must proportion according to the bulk mass fraction. That is,

$$\epsilon_n=Y_{l,n0};\quad n=1,\ldots,N-2. \tag{36}$$

Now, Eq. (19) can be recast as

$$\frac{L+c_l[T_S-T_{l0}]+\sum_{k=1}^{N-2}Y_{l,k0}[h_{k,\infty}-h_{k,S}]}{L+c_l[T_S-T_{l0}]}=\left[\frac{Y_{l,n0}}{Y_{l,n0}-Y_{n,S}}\right]^{1/Le_{\epsilon,n}},\quad n=1,\ldots,N-2, \tag{37}$$

where any value of n may be used. This equation may be regarded as a constraint on the interface temperature T_S which can be employed to determine that temperature.

Then, if all gas-phase mass diffusivities are identical, Eq. (23) yields that

$$\frac{Y_{n,S}}{\sum_{k=1}^{N-2}Y_{k,S}}=Y_{l,n0},\quad n=1,\ldots,N-2. \tag{38}$$

Combining Eq. (38) with (13), we obtain

$$Y_{\mathrm{l},n0} = \frac{W_n X_{\mathrm{l},n,\mathrm{S}} \sum_{k=1}^{N} (Y_{k,\mathrm{S}}/W_k)}{p \sum_{k=1}^{N-2} Y_{k,\mathrm{S}}} \mathrm{e}^{L_n/RT_{\mathrm{b},n}} \mathrm{e}^{-L_n/RT_{\mathrm{S}}}, \quad n = 1, \ldots, N-2. \tag{39}$$

Now, the above $N-2$ relations will yield the following $N-3$ relations after common quantities are eliminated:

$$X_{\mathrm{l},n,\mathrm{S}} = X_{\mathrm{l},1,\mathrm{S}} \frac{\mathrm{e}^{L_1/RT_{\mathrm{b},1}} \mathrm{e}^{-L_1/RT_{\mathrm{S}}}}{\mathrm{e}^{L_n/RT_{\mathrm{b},n}} \mathrm{e}^{-L_n/RT_{\mathrm{S}}}} \frac{W_1 Y_{\mathrm{l},n0}}{W_n Y_{\mathrm{l},10}}, \quad n = 2, \ldots, N-2. \tag{40}$$

These equations together with $\sum_{k=1}^{N-2} X_{\mathrm{l},k,\mathrm{S}} = 1$ form $N-2$ linear relations that yield the $X_{\mathrm{l},n,\mathrm{S}}$ values. They can be solved by an iteration process. A value of T_{S} is guessed. Use Eq. (40) to obtain the $X_{\mathrm{l},n,\mathrm{S}}$ values. Once $X_{\mathrm{l},n,\mathrm{S}}$ and T_{S} are known, Eq. (13) together with $\sum_{k=1}^{N} Y_{k,\mathrm{S}} = 1$ and a statement about the mass ratio of oxygen to nitrogen at the interface yields the gas mass fractions $Y_{n,\mathrm{S}}$ at the interface. Note that, since the gas-phase mass diffusivities were taken to be identical, the mass ratio of oxygen to nitrogen is identical throughout the field to the imposed ratio at infinity. Now, use Eq. (37) to obtain the next value of temperature T_{S}. Cycle through these steps until converged solutions result.

7.3. Slow-vaporization limit

In this limit, the times for liquid-phase heat and mass-diffusion are very short compared to the droplet lifetime. Therefore, we approximate that temperature T_{l} and concentrations $X_{\mathrm{l},n}$ are instantaneously uniform across the liquid although time-varying. We will simplify our task by assuming that all gas-phase diffusivities are equal. The values of ϵ_n and $Y_{n,\mathrm{S}}$ are given as functions of T_{l} and $X_{\mathrm{l},n}$ by Eqs. (13) and (23) together with the condition that $\sum_{k=1}^{N} Y_{k,\mathrm{S}} = 1$ and a statement about the mass ratio of oxygen and nitrogen.

The liquid mole fractions $X_{\mathrm{l},n} = N_n/N$ where N_n and $N = \sum_{k=1}^{N-2} N_k$ are the moles of liquid species n in a droplet and the total number of moles in the liquid droplet, respectively. From conservation of mass principles for the liquid in the droplet, we can form the differential equations

$$-\frac{1}{4\pi R \frac{\epsilon_n}{W_n} \eta_{\mathrm{A}}} \frac{\mathrm{d}N_n}{\mathrm{d}t} = \frac{\overline{\lambda}}{c_{p,\epsilon}} \ln(1 + B_{\mathrm{H},\epsilon}) = \overline{\rho D_n} \ln(1 + B_{\mathrm{M},n}), \quad n = 1, \ldots, N-2 \tag{41}$$

and

$$-\frac{1}{4\pi R \left[\sum_{k=1}^{N-2} \frac{\epsilon_k}{W_k}\right] \eta_{\mathrm{A}}} \frac{\mathrm{d}N}{\mathrm{d}t} = \frac{\overline{\lambda}}{c_{p,\epsilon}} \ln(1 + B_{\mathrm{H},\epsilon}) = \overline{\rho D_n} \ln(1 + B_{\mathrm{M},n}). \tag{42}$$

So, prescription of initial values for R, N_n, and N allows simultaneous integration of the first-order ordinary differential Eqs. (30), (41), and (42).

The energy-balance for a uniform droplet temperature can be obtained using Eq. (34) which yields

$$\frac{\mathrm{d}T_{\mathrm{l}}}{\mathrm{d}t} = -\frac{3\dot{R}}{c_{\mathrm{l}} R} \left[\frac{\sum_{k=1}^{N-2} \epsilon_k (h_{k,\infty} - h_{k,\mathrm{S}})}{(1 + B_{\mathrm{M},n})^{1/Le_{\epsilon,n}} - 1} - \sum_{k=1}^{N-2} \epsilon_k L_k \right]. \tag{43}$$

The prescription of an initial value for liquid temperature allows the simultaneous solution of this first-order ordinary differential equation with the above equations.

The diffusion of mass in common liquids is much slower than the heat-diffusion; so, a decent approximation can be achieved by replacing the differential Eq. (43) by the relation (26) which yields the wet-bulb temperature. That is, the time-varying composition of the liquid will be the controlling factor in determining the liquid temperature.

7.4. Other asymptotic behavior

Since the Schmidt number is an order of magnitude larger than the Prandtl number for common liquids, other asymptotic situations can become of practical interest. For example, a situation might arise where the temperature is uniform or nearly uniform through the droplet interior while spatial gradients in the liquid mole and mass fractions still exist. The table indicates which combination of equations would be used in various situations. As described above for the liquid-phase, the thermal behavior or the mixing behavior can be considered as one of three possible situations: a nearly uniform but time-varying scalar field, a transient field, or a quasi-steady behavior with a thin diffusive layer near the interface. The various combinations of these three cases for each scalar produce nine cases shown in Table 1. Three cases are not practical because they imply that mass-diffusion is faster than heat-diffusion in the liquid. Three other cases have been discussed earlier in this Section. There are three new combinations where the slower mass-diffusion compared to heat-diffusion allows a distinction from the cases discussed in the three previous subsections. The governing equations for those situations are listed in Table 1.

Table 1
Comparison and feasibility of various liquid-phase heating models

Case	Uniform $Y_{\mathrm{l},n}$	Transient $Y_{\mathrm{l},n}$	Quasi-steady $Y_{\mathrm{l},n}$
Uniform T_{l}	See Section 7.3	Eqs. (11), (13), (21) and (33); Conditions 3, 4, 6 of (34); and (22) or (43)	Eqs. (36), (38)–(40) and (22) or (43)
Transient T_{l}	Not practical	See Section 7.1	Eq. (32); conditions 1, 2, 5 of 34, 19, and 35
Quasi-steady T_{l}	Not practical	Not practical	See Section 7.2

8. Computational results

The theory has been developed for a very general configuration and for an arbitrary number of species in the liquid-phase. Here, for the sample calculations, we choose an eight-droplet array with triple symmetry; in particular, the droplets are at the corners of an abstract cube so spacing between droplets is uniform. The liquid droplets have the same initial size; initial temperature; and initial composition, a blend of heptane, octane, and decane. Droplet spacing is ten times the initial droplet radius. Ambient pressure is one atmosphere. Ambient temperatures and liquid-phase mixture ratios will be varied.

In the calculation, data and equations for thermodynamic and transport properties are given in the literature [17–19]. The droplets vaporize in the air where nitrogen dominates, so the mass diffusivities in the gas-phase are determined as the binary diffusivities of each species in nitrogen which vary both in space and time. In the liquid-phase, there is no species that dominates, and the mass diffusivity of one species is determined by weighting its binary mass diffusivities specifically in other two species based on their relative mass fraction. The binary diffusivities in the liquid-phase are given by semi-empirical equations.

The scalar properties in the gas-phase are solved in terms of normalized mass-flux potential Φ which varies from 0 to 1. A grid size of 0.01 in Φ is sufficiently small. The errors of integration (evaluated as the changes of average gas-phase scalars when the grid side reduces to half) are below 0.1%. During the transient behavior, the profile changes for liquid-phase scalars are large near the surface; so, smaller mesh size there is needed to calculate the liquid-phase more accurately. A mesh size of 1/800 of the normalized radius makes the integration errors (evaluated as the deviation of the cumulative mass vaporized for one species from the change of mass of this species in the liquid) below 1% and results in error decrease with time. The Forward-Time-Center-Spacing (FTCS) scheme is used and the discrete governing equations and boundary conditions in the liquid-phase are solved using a tridiagonal-matrix algorithm. The forward-time scheme is also used for the slow-vaporization limit. Five thousand time steps in the whole lifetime of droplets are enough to ensure a satisfying accuracy.

Fig. 1 shows the change of surface temperature and mass fraction of heptane, octane and decane at the liquid surface with time in transient behavior for both interactive and isolated-droplets. The surface temperature rises sharply at the beginning and then increases more and more gently, before the droplet is gone. At the liquid surface, the mass fraction of the most volatile component heptane drops steadily for a long time and then remains nearly constant due to the achieved balance between heptane's volatility and its large gradient of concentration in the liquid near the surface. The isolated-droplets vaporize faster and have greater rates of change of surface scalars than interactive droplets. The values for surface scalars for interactive and isolated-droplets come very close to each other near the end of the lifetime when the droplet spacing is rather large compared to the droplet radius.

Addition of some non-volatile species to the liquid is known to elevate the boiling point of the volatile species. Based on Raoult's law, the components' boiling point in the mixture is given by this equation: $1/T_{bi} - 1/T_{bi,\mathrm{pure}} = R \cdot \ln(X_{i,l})/L_i$. This relationship indicates that T_{bi} can be greater than $T_{bi,\mathrm{pure}}$; that is, the boiling point of a species in a mixture will exceed its boiling point in pure form. The boiling points of heptane, octane and decane in pure form are 371.58 K, 398.83 K and 447.3 K specifically. Fig. 2a shows that the actual boiling points of all the three species are greater than their values in pure form. The actual boiling points of heptane and octane at the liquid surface increase with time due to their greater volatility and subsequently decrease in their mole fractions near the liquid surface, while the actual boiling point of decane decreases due to its lower volatility and increase of mole fraction near the liquid surface. This elevation of boiling point means that the temperature at any location in the

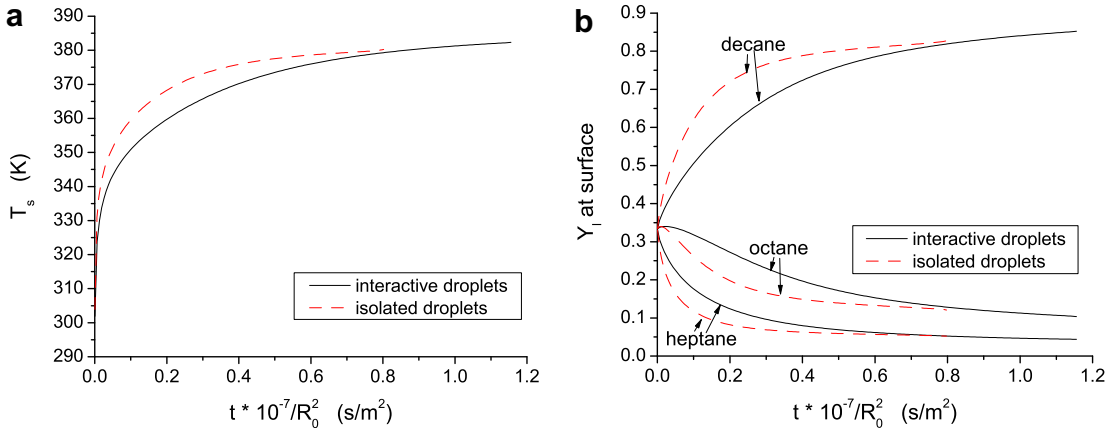

Fig. 1. Surface temperature and species mass fraction at the liquid surface in transient behavior for both interactive and isolated droplets, at the ambient temperature 2000 K, and initial mass fraction for heptane, octane and decane: 1/3, 1/3, 1/3.

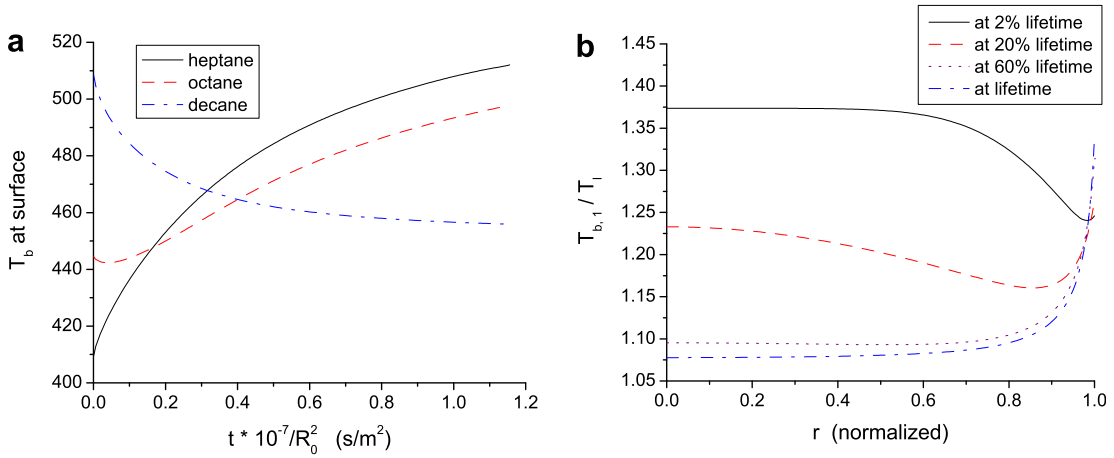

Fig. 2. Boiling point during the transient behavior, at the ambient temperature 2000 K, and initial mass fraction for heptane, octane and decane: 1/3, 1/3, 1/3. (a) Actual boiling point at the surface. (b) Profiles of actual boiling point over liquid temperature for heptane at different times.

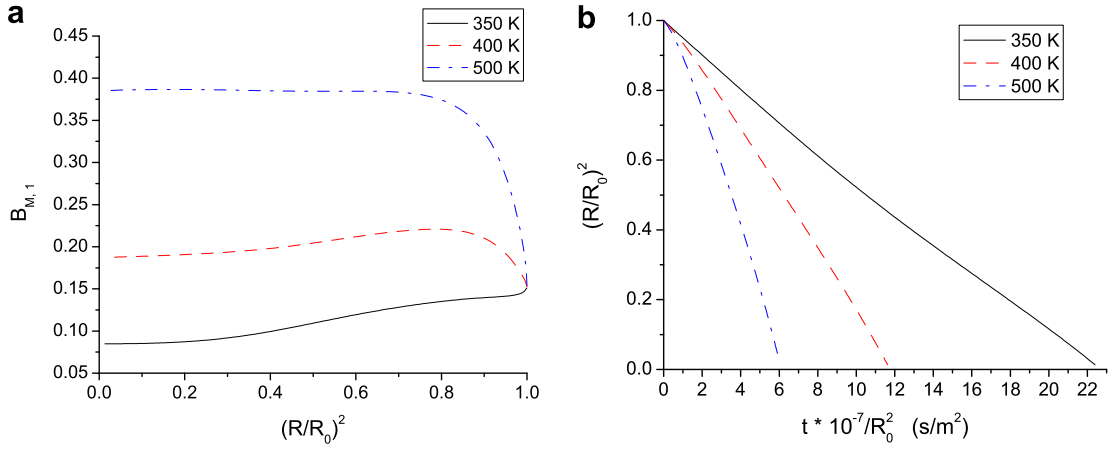

Fig. 3. Comparisons of $B_{M,1}$ vs. $(R/R_0)^2$ and $(R/R_0)^2$ vs. t curves at different ambient temperature during the transient behavior, with identical initial mass fraction for heptane, octane and decane.

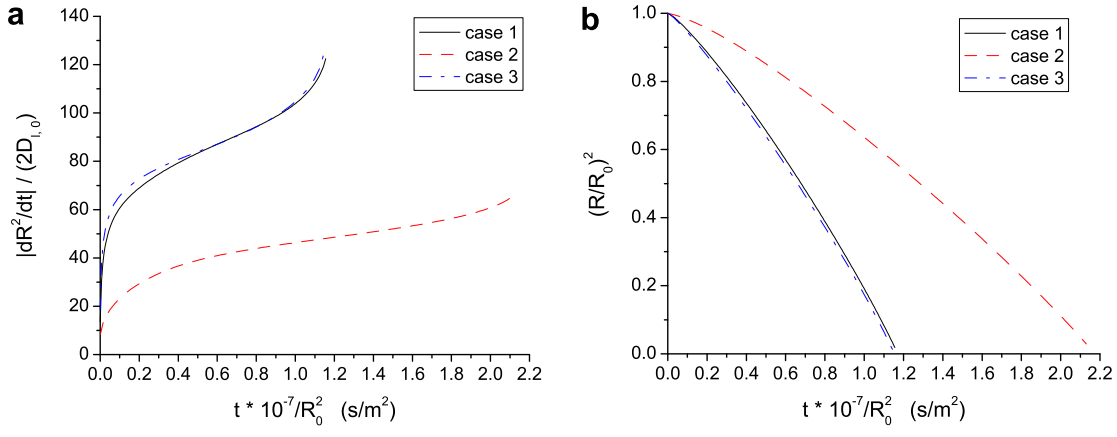

Fig. 4. Normalized vaporization rate $(|dR^2/dt|/(2D_{l,0}) = \dot{m}/(4\pi\rho_l R D_{l,0})$, $D_{l,0} = 4 \times 10^{-9}$ m^2/S) and normalized radius squared during the transient behavior in three cases: 1–2000 K (ambient temperature), 1/3, 1/3, 1/3 (initial mass fraction for heptane, octane and decane); 2–1000 K, 1/3, 1/3, 1/3; 3–2000 K, 2/3, 1/6, 1/6.

droplet will not exceed any component's actual boiling point at that location at any time. Thus, no interior gasification will occur, even if the boiling temperature for a pure substance is exceeded. Fig. 2b applies to the case of heptane. It shows that the liquid temperature only exceeds heptane's boiling point in pure form after sometime.

During the transient behavior, the increasing η_A and normally increasing $B_{M,n}$ and surface temperature tend to make the rate of decrease of radius squared become larger with time (i.e. tend to make $(R/R_0)^2$ vs. t curve convex). This is consistent with our knowledge of single-component droplet arrays [1,12]. However, when the ambient temperature is very low, $B_{M,n}$ may decrease with time due to a strong distillation effect, and the $(R/R_0)^2$ vs. t curve may consequently become concave (see the 350 K case in Fig. 3).

Higher ambient temperature leads to faster vaporization rate. Fig. 4 shows that the normalized vaporization rate at ambient temperature 2000 K is nearly two times that at 1000 K. The mixture with greater fractions of the more volatile components has faster radius squared rate of change and thus has a shorter droplet lifetime. We also examined

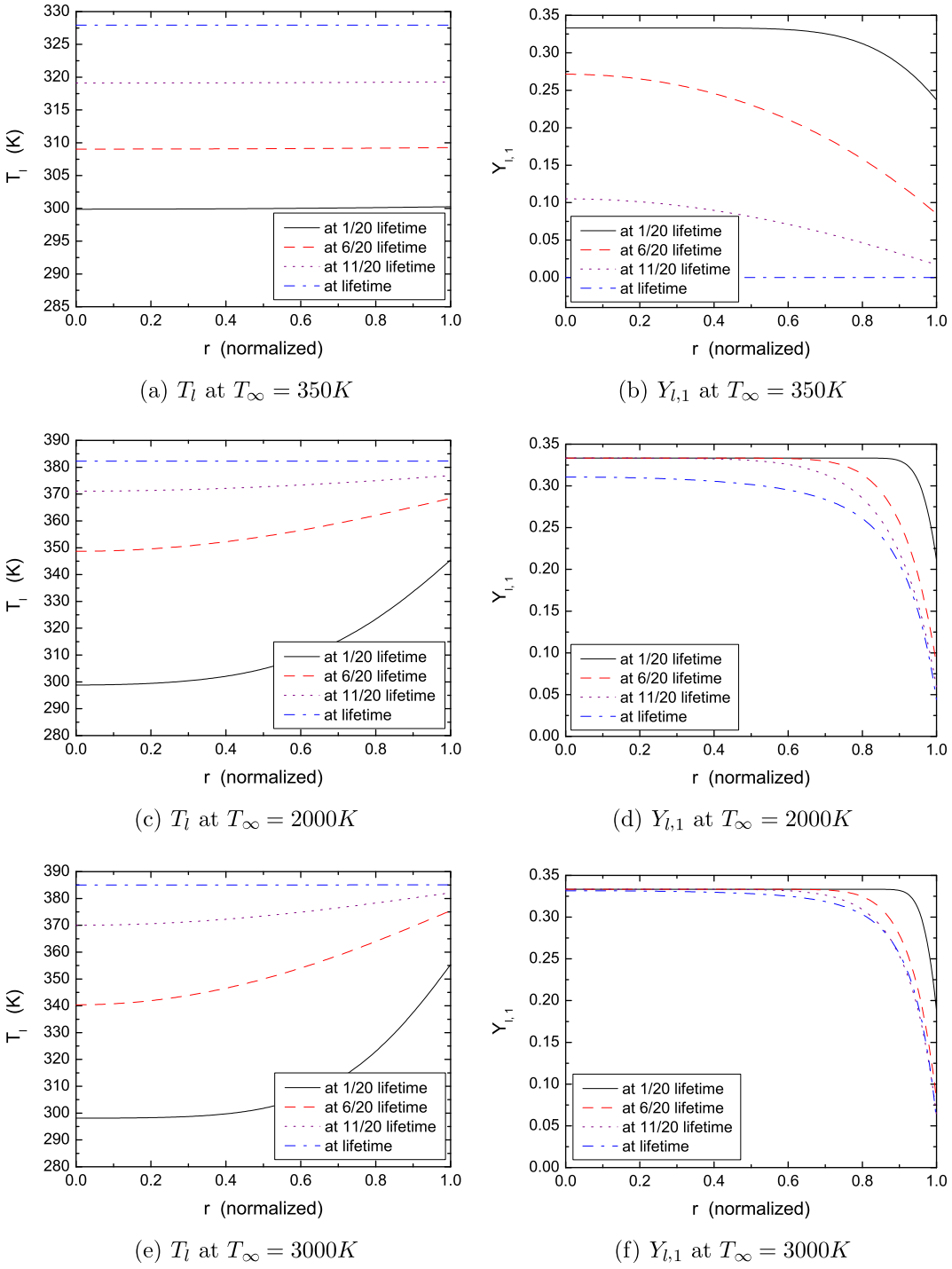

(a) T_l at $T_\infty = 350K$ (b) $Y_{l,1}$ at $T_\infty = 350K$

(c) T_l at $T_\infty = 2000K$ (d) $Y_{l,1}$ at $T_\infty = 2000K$

(e) T_l at $T_\infty = 3000K$ (f) $Y_{l,1}$ at $T_\infty = 3000K$

Fig. 5. Profiles of temperature and heptane mass fraction in the liquid-phase during the transient behavior, with identical initial mass fraction for heptane, octane and decane.

transient heating and vaporization for an artificial liquid with temporally constant properties that were averaged values for a mixture of heptane, octane and decane and compare it with the actual mixture of the three species with identical initial mass fraction. The artificial liquid with equal weighting of the three components has faster radius squared rate of change than the actual mixture, because the mass fractions of the more volatile components become smaller than their initial value in the process of the vaporization of the mixture and thus less weighting should be put on the more volatile components in order to have a radius squared rate of change closer to the value for the actual mixture.

During the transient behavior, there is heat conduction and species diffusion inside the droplets. Fig. 5a–f shows

Table 2
Parameters at equilibrium for pure octane at the ambient temperature 2000 K and 3000 K: surface temperature (K), octane mass fraction at gas surface, vaporization rate divided by droplet radius and interaction-isolated rate ratio (Kg/(m s)), effective latent heat (J/Kg) and time divided by initial radius squared (s/m^2) when $(R/R_0)^2 = 0.01$

		T_S	Y_S	$\dot{m}/(R \cdot eta)$	L_{eff}	$t_{life} \times 10^{-7}/R_0^2$
$T_\infty = 2000$ K	Fast-vaporization limit	354.73	0.5895	4.239E−3	4.317E+5	1.1715
	Transient behavior	357.77	0.6224	4.669E−3	3.050E+5	1.1401
$T_\infty = 3000$ K	Fast-vaporization limit	360.04	0.6466	6.086E−3	4.436E+5	0.8160
	Transient behavior	362.77	0.6755	6.580E−3	3.051E+5	0.7974

The values for transient behavior are applied when $(R/R_0)^2 = 0.1$.

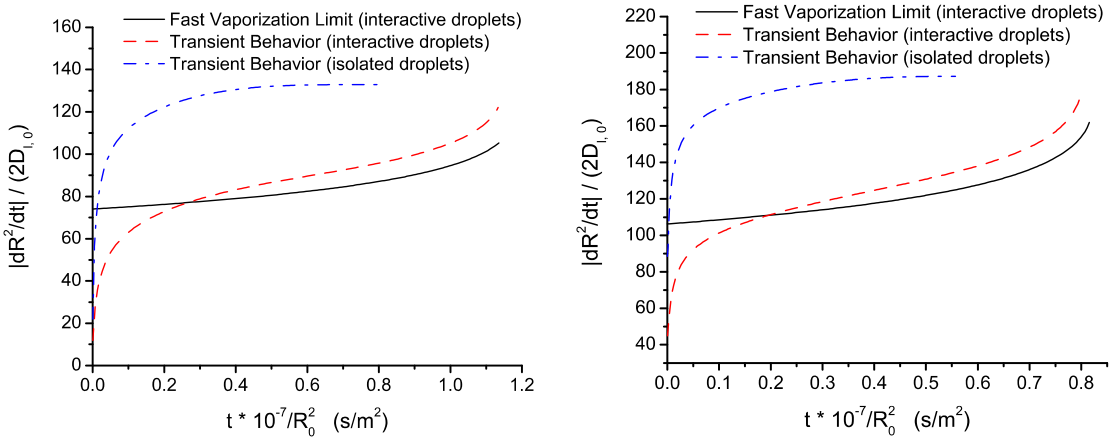

(a) $T_\infty = 2000K$ (b) $T_\infty = 3000K$

Fig. 6. Comparisons of normalized vaporization rate in the fast-vaporization limit and transient behavior of both interactive and isolated-droplets, for pure octane.

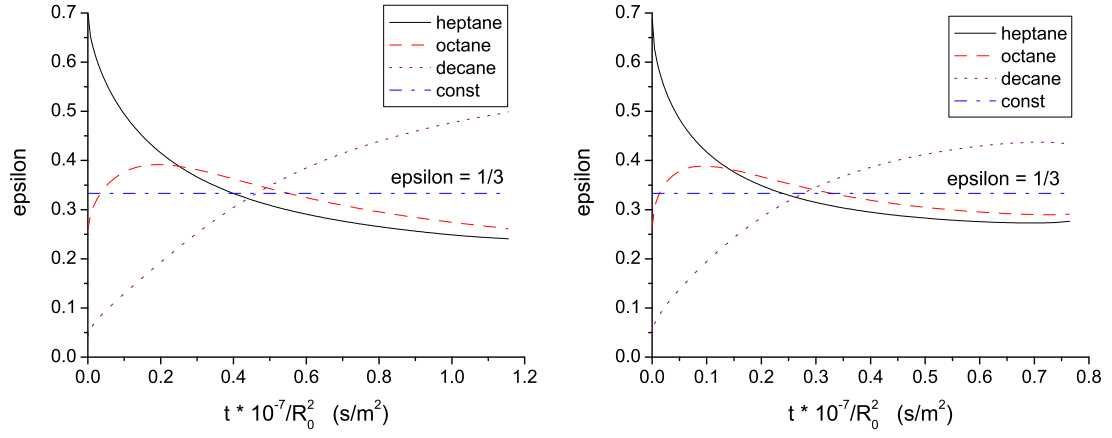

(a) $T_\infty = 2000K$ (b) $T_\infty = 3000K$

Fig. 7. Mass-flux fraction during the transient behavior compared to the fast-vaporization limit, with identical initial mass fraction for heptane, octane and decane.

the profiles of interior temperature and heptane mass fraction at different times in the droplet lifetime. These profiles change with time while the changes of surface temperature and surface composition become slower with time. As liquid-phase heat conduction is much faster than mass-diffusion, the temperature becomes nearly uniform and constant after some time while the profiles of species mass fraction still vary. Lower ambient temperature always leads to more uniform profiles because it results in longer lifetime and allows more time for heat and species diffusion in the droplets. For 350 K ambient temperature, the temperature profiles are nearly uniform all the time but the mass fraction profiles are not; so, the slow-vaporization limit is not strictly satisfied even at low ambient temperature 350 K. For 3000 K ambient temperature, the temperature and mass fraction profiles become steeper but still do not produce a sufficiently thin diffusion layer to satisfy strictly the fast-vaporization limiting conditions.

In the single-component case, the droplets will reach a fixed equilibrium point when surface temperature and fuel mass fraction at the gas surface are kept constant. We calculated parameters at equilibrium for the single-component of octane in the fast-vaporization limit and transient behavior case at both 2000 K and 3000 K ambient temperature. In Table 2, T_S, Y_S and $\dot{m}/(R \cdot eta)$ are greater, after the initial start-up portion of the transient behavior with high ambient temperature, than given by the formula for the fast-vaporization limit. The transient behavior has higher initial heating rate (i.e., higher initial L_{eff}) which eventually results in higher liquid temperatures and thus yields a lower effective latent heat L_{eff} at later times. Fig. 6 shows that the normalized vaporization rate for the interactive droplet in the fast-vaporization limit gives a lower vaporization rate after start-up.

In the multicomponent case, the mass-flux fraction of each component equals its initial mass fraction in the fast-vaporization limit. Fig. 7 shows the change of mass-flux fraction with time during the transient behavior, compared to the constant value in the fast-vaporization limit. The curves at the ambient temperature 3000 K are closer to the constant value 1/3 than at 2000 K, but still have an apparent difference, because the fast-vaporization limit is still not well approached as shown in Fig. 5e and f. Fig. 8 shows the difference in the normalized vaporization rate between the fast-vaporization limit and transient behavior at the ambient temperature 3000 K.

The slow-vaporization limit is suitable when the ambient temperature is low and vaporization rate is small compared to heat conduction and species diffusion rates in the liquid-phase. For a single liquid species, there is only heat conduction in the liquid-phase and the difference in the effective latent heat leads to the difference of vaporization rate of the slow-vaporization limit compared to that for the calculation of the transient behavior: at first, the slow-vaporization model gives a smaller vaporization rate, later a greater rate, and finally the rates become nearly identical. See the results for pure liquid octane in Fig. 9a. When the ambient temperature becomes very small, the difference in vaporization rate for these two cases can be neglected (Fig. 9b) due

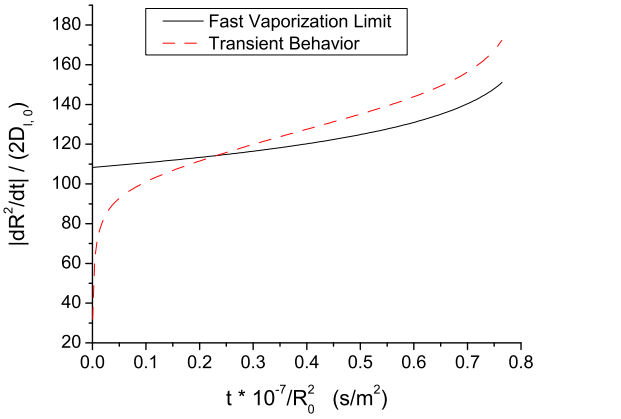

Fig. 8. Comparison of normalized vaporization rate between the fast-vaporization limit and transient behavior, at the ambient temperature 3000 K and identical initial mass fraction for heptane, octane and decane.

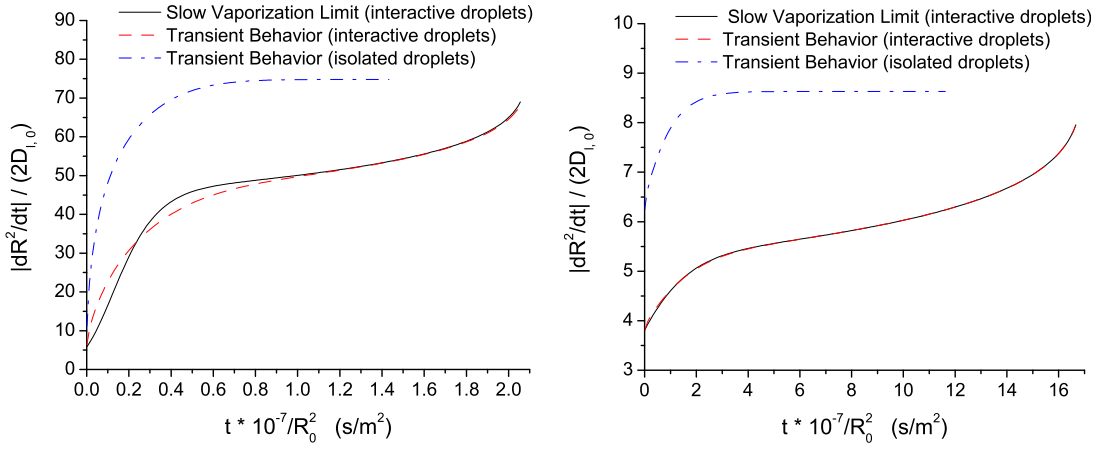

(a) $T_\infty = 1000K$ (b) $T_\infty = 350K$

Fig. 9. Comparisons of normalized vaporization rate between the slow-vaporization limit and transient behavior, for single octane.

to the small ratio of vaporization rate to heat conduction rate.

For multicomponent droplets, there is also species diffusion in the liquid-phase, and the infinitely fast species diffusion rate in the slow-vaporization limit makes the more volatile components vaporize primarily in the earlier period without much remaining for the rest compared to a much more gentle change of the mass-flux fraction of each component in the transient behavior calculation (Fig. 10d). Because species diffusion rate is much smaller than heat conduction rate in the liquid-phase, at a low temperature 350 K the ratio of vaporization rate to species diffusion rate is still not sufficiently small and thus there are still apparent differences in the curves of mass-flux fraction for the slow-vaporization limit and transient behavior case (Fig. 11d). At the ambient temperature 1000 K, the vaporization rate is not small compared to both heat conduction rate and species diffusion rate; so, the difference between heat conduction and species diffusion jointly leads to a difference in the vaporization rate for the slow-vaporization limit and transient behavior case (Fig. 10b). At the ambient temperature 350 K, the vaporization rate is small compared to heat conduction rate but not compared to species diffusion rate; so, the difference of species diffusion primarily leads to the difference in the vaporization rate for the slow-vaporization limit and transient behavior case (Fig. 11b).

When the droplet spacing is changed from ten times the initial droplet radius to five times the initial droplet radius, the vaporization rate becomes smaller due to increased interaction effect and subsequently smaller interactive-isolated vaporization ratio (Fig. 12a and b). The values of surface scalars vary monotonically with droplet spacing; see Figs. 1 and 12c and d. The isolated-droplet case is the case for infinite droplet spacing. The 10-radii-spacing values lie between the isolated-droplet and five-radii-spacing cases.

Quantitative experimental results are not available for vaporizing multicomponent droplet arrays. For isolated-droplets, some experimental evidence is available for bi-component blends but none exists for tri-component blends. Randolph et al. [20] have studied binary blends of hexadecane with other lighter alkanes. The experimental results show that the more volatile component vaporizes faster than the less volatile result which qualitatively agrees with our computations. The computational results have a good fit with the experimental results (see Fig. 13) if the

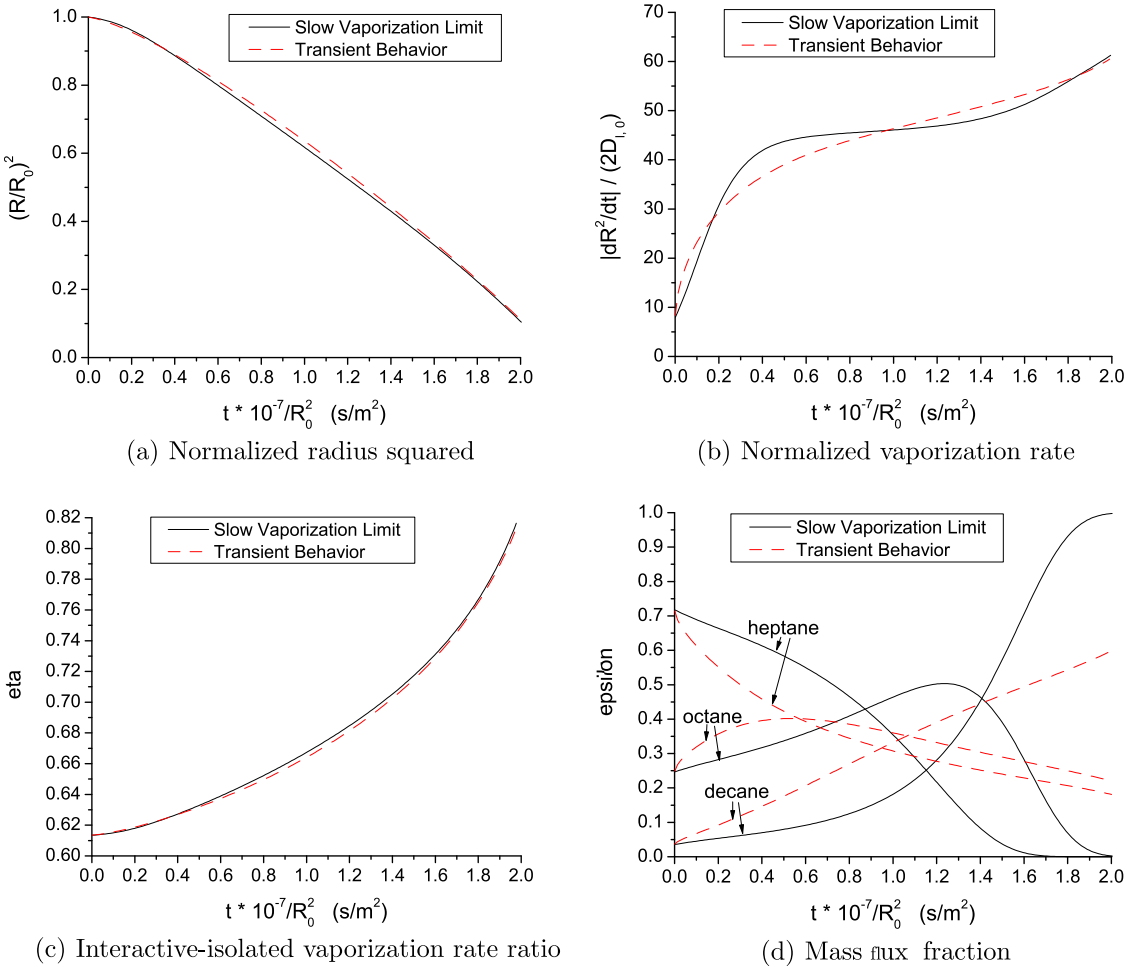

(a) Normalized radius squared

(b) Normalized vaporization rate

(c) Interactive-isolated vaporization rate ratio

(d) Mass flux fraction

Fig. 10. Comparisons between the slow-vaporization limit and transient behavior, at the ambient temperature 1000 K and initial mass fraction for heptane, octane and decane: 1/3, 1/3, 1/3.

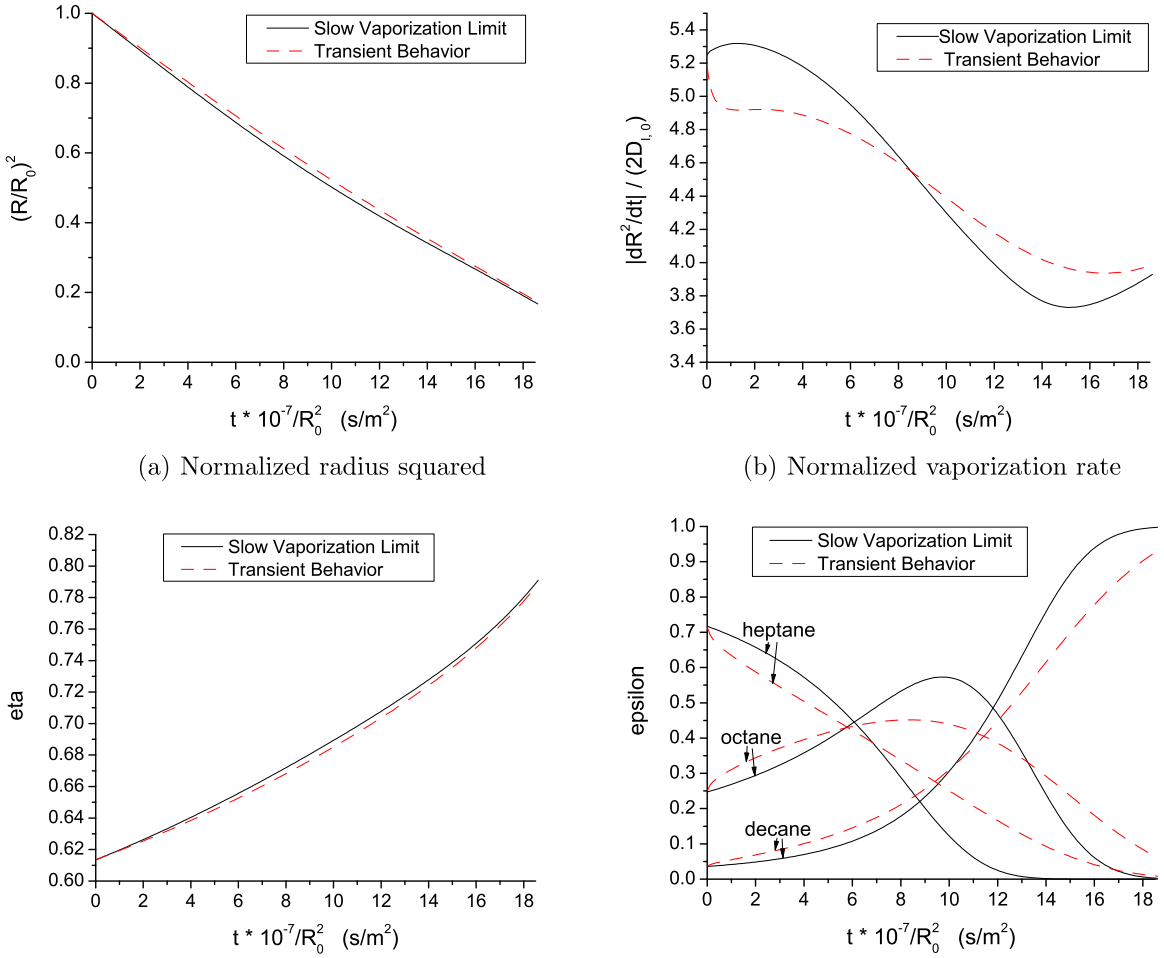

Fig. 11. Comparisons between the slow-vaporization limit and transient behavior, at the ambient temperature 350 K and initial mass fraction for heptane, octane and decane: 1/3, 1/3, 1/3.

liquid mass diffusivity is taken to have a value about twice its original value. The bi-component calculations of Randolph et al. required a similar artificial adjustment to match their experimental data. There are two possible explanations for the need for adjustment. Since their experiment involved some relative motion for the droplets, internal liquid circulation might have hastened the mixing rate and effective diffusivity. Also, time counting in the experiment did not begin until ignition so some shift of the experimental data to the right would occur in an accurate time plot for Fig. 13, creating a better fit with theory.

9. Concluding remarks

A generalized theory for multicomponent-liquid–fuel vaporization in an arbitrary geometrical configuration (e.g., arbitrary number of droplets with arbitrary sizes and spacings) with a non-unitary Lewis number is obtained under the assumptions of uniform liquid surface temperature and no forced or natural convection. It extends previous work by Sirignano [4] and Imaoka and Sirignano [1–3]. Solutions are obtained as functions of the mass-flux potential, recasting a three-dimensional scalar field as a one-dimensional solution. The mass-flux potential is a solution of Laplace's equation in three dimensions. Mass-flux-weighted enthalpies and specific heats are more useful than mass-weighted quantities. A revised definition of the Lewis number is required because of the mass-flux-weighted specific heats. The correct (i.e., natural) method for averaging transport properties over the field is demonstrated to be based upon an integration of the reciprocal value over the mass-flux potential.

A useful integral relation (24) that constrains liquid surface temperature and heat flux has been developed. This can serve as a boundary condition on the liquid-phase heat-diffusion equation. A new heat-transfer number $B_{H\epsilon}$ is constructed as a modification of Spalding's heat-transfer number. A direct relation between the mass-transfer number B_M and this new number only occurs when the modified Lewis number has the same constant value throughout the field. This relationship for $L_{eff}(T_S)$ does not vary with geometry but rather has a more universal character.

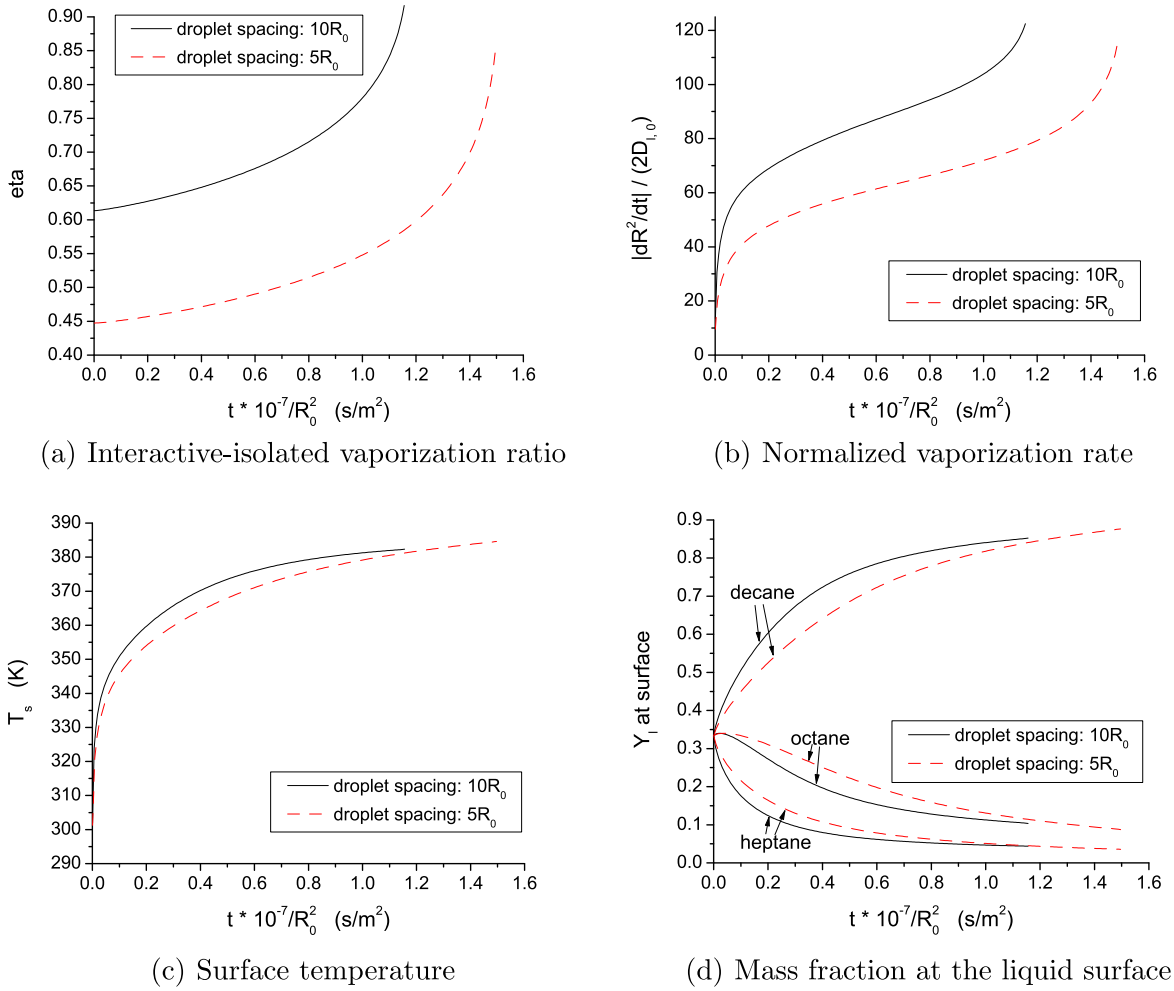

Fig. 12. Comparisons between cases of $10R_0$ and $5R_0$ droplet spacing during the transient behavior, with ambient temperature 2000 K and identical initial mass fraction for heptane, octane and decane.

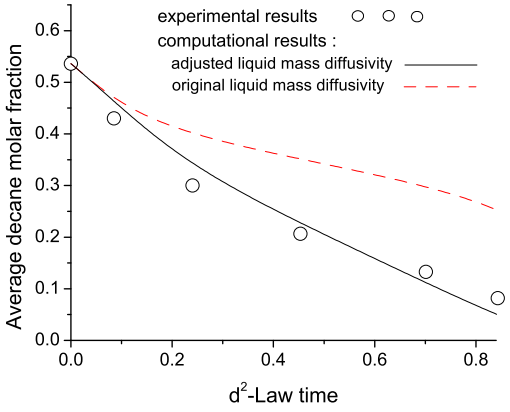

Fig. 13. Temporal variation of the average decane molar fractions for mixtures of hexadecane and decane undergoing vaporization at about 1020 K.

Unsteady diffusion in the liquid-phase have been analyzed. Various asymptotic cases have been studied where heat- and mass-diffusion times become large or small compared to a droplet lifetime or where one diffusion time becomes short compared to the other. The uniform-surface-temperature assumption is critical since a certain symmetry for all droplets is implied in the transient heating case. Only for the quasi-steady case where a wet-bulb temperature has been reached, can the surface temperatures be identical for all droplets in any configuration. The mass-transfer number $B_{M,n}$, the fuel-vapor mass fractions at the interface $Y_{n,S}$, and the vaporization rate are shown to vary strongly with surface temperature. $B_{M,n}$ and $Y_{n,S}$ do not directly depend on transport properties. However, the temporal behavior of surface temperature depends on transport properties; so, an indirect impact on $B_{M,n}$ and $Y_{n,S}$ will occur.

The Marangoni convection has not been considered in this problem where combustion does not occur. Computations (Pages 63-4 of Ref. [12]) have shown that it can be important when a flame is in the vicinity of the droplet. With a flame surrounding an array of droplets, the flame would be standing at a greater distance from the droplets; so, the importance of surface tension for droplet group or array burning remains an open question. If the surface tension were important, it would make the temperature along the droplet surface more uniform, justifying an important assumption in our analysis.

Sample calculations are performed using eight droplets in a cubic array with a liquid that is a blended mixture of heptane, octane, and decane. Various ambient temperatures and liquid-phase mixture ratios are examined. The transport properties in both gas and liquid-phase are variable. The changes of surface scalars, radius squared, vaporization rate, gas-phase scalar profiles, and liquid-phase scalar profiles are determined for the transient behavior. Boiling points for each component are elevated in the blend compared to the boiling temperatures for pure substances. The boiling point for a substance in a liquid blend is higher than its boiling point in pure form. Consequently, liquid temperatures do exceed the pure form boiling point of the most volatile substance in some portion of the liquid after heating.

Comparisons are made amongst the results for the various liquid-diffusion models: transient behavior, the fast-vaporization limit, and the slow-vaporization limit. Specifically, comparisons are made at high or low ambient temperature. Some significant differences between the fast-vaporization asymptotic results and the more accurate transient diffusion computations occur even at ambient temperatures as high as 3000 K. Similarly, some differences between the slow-vaporization asymptotic results and the more accurate transient diffusion computations are found even at ambient temperatures as low as 350 K. For multicomponent droplets, the fast-vaporization-limit model is very poor at predicting the vaporization rates of individual liquid components, even at ambient temperatures of 3000 K. During the initial heating period, it poorly predicts overall mass vaporization rate. At low temperatures of 350 K, the slow-vaporization limit gives acceptable predictions for the single-component case but not for the multicomponent case. Droplet vaporization and heating rates decreased as initial droplet spacing decreased. The largest values occurred for the isolated-droplet case.

Imaoka and Sirignano [3] examined the effects of non-uniform initial droplet size and spacing for single-component liquids. The results correlated well with the uniform size and spacing results if certain averaged size and spacing are used. It is suspected that a similar result can be found for multicomponent liquid droplets; this can be viewed as a candidate for future work.

References

[1] R.T. Imaoka, W.A. Sirignano, Vaporization and combustion in three-dimensional droplet arrays, Proc. Combust. Inst. 30 (2004) 1981–1989.
[2] R.T. Imaoka, W.A. Sirignano, A generalized analysis for liquid–fuel vaporization and burning, Int. J. Heat Mass Transfer 48 (2005) 4342–4353.
[3] R.T. Imaoka, W.A. Sirignano, Transient vaporization and burning in dense droplet arrays, Int. J. Heat Mass Transfer 48 (2005) 4354–4366.
[4] W.A. Sirignano, Liquid–fuel burning with non-unitary Lewis number, Combust. Flame 148 (2007) 177–186.
[5] M. Labowsky, The effects of nearest neighbor interactions on the evaporation rate of cloud particles, Chem. Eng. Sci. 31 (1976) 803–813.
[6] M. Labowsky, A formalism for calculating the evaporation rates of rapidly evaporating interacting particles, Combust. Sci. Technol. 18 (1978) 145–151.
[7] M. Labowsky, Calculation of the burning rates of interacting fuel droplets, Combust. Sci. Technol. 22 (1980) 217–226.
[8] A. Umemura, S. Ogawa, N. Oshima, Analysis of the interaction between two burning droplets, Combust. Flame 41 (1981) 45–55.
[9] A. Umemura, S. Ogawa, N. Oshima, Analysis of the interaction between two burning fuel droplets with different sizes, Combust. Flame 43 (1981) 111–119.
[10] T.A. Brzustowski, E.M. Twardus, S. Wojcicki, A. Sobiesiak, Interaction of two burning fuel droplets of arbitrary size, AIAA J. 17 (1979) 1234–1242.
[11] E.M. Twardus, T.A. Brzustowski, The interaction between two burning fuel droplets, in: Fifth International Symposium on Combustion Processes, vol. 8, Krakow, Poland, 1977.
[12] W.A. Sirignano, Fluid Dynamics and Transport of Droplets and Sprays, Cambridge University Press, New York, 1999.
[13] H.H. Chiu, H.Y. Kim, E.J. Croke, Internal group combustion of liquid droplets, in: Nineteenth Symposium (International) on Combustion/The Combustion Institute, vol. 19, 1982, pp. 971–980.
[14] J.O. Hirschfelder, C.F. Curtiss, R.B. Bird, Molecular Theory of Gases and Liquids, John Wiley, New York, 1954.
[15] M.M. El Wakil, R.J. Priem, H.J. Brikowski, P.S. Meyers, O.A. Uyehara, Experimental and calculated temperature and mass histories of vaporizing fuel drops, in: NASA TN 3490, 1954.
[16] C.K. Law, H.K. Law, Quasi-steady diffusion flame theory with variable specific heats and transport coefficients, Combust. Sci. Technol. 12 (1976) 207–216.
[17] W.C. Gardiner, Combustion Chemistry, Springer Verlag, New York, 1984.
[18] S. Bretsznajder, Prediction of Transport and Other Physical Properties of Fluids, Pergamon Press, 1971.
[19] C.L. Yaws, Chemical Properties Handbook, McGraw Hill, 1999.
[20] A.L. Randolph, A. Makino, C.K. Law, Liquid-phase diffusional resistance in multicomponent droplet gasification, Proc. Combust. Inst. 21 (1988) 601–608.